Redox Biology 14 (2018) 549–556

Contents lists available at ScienceDirect

Redox Biology

journal homepage: www.elsevier.com/locate/redox

Research Paper

Redox-sensitive GFP fusions for monitoring the catalytic mechanism and inactivation of peroxiredoxins in living cells

Verena Staudacher[a,b,c], Madia Trujillo[c], Tim Diederichs[d], Tobias P. Dick[e], Rafael Radi[c,*,1], Bruce Morgan[d,*,1], Marcel Deponte[a,b,**,1]

[a] University of Kaiserslautern, Erwin-Schrödinger-Straße 54, D-67663 Kaiserslautern, Germany
[b] Department of Parasitology, Ruprecht-Karls University, Im Neuenheimer Feld 324, D-69120 Heidelberg, Germany
[c] Departamento de Bioquímica, Facultad de Medicina and Center for Free Radical and Biomedical Research, Universidad de la República, Avda. General Flores 2125, 11800 Montevideo, Uruguay
[d] Department of Biology/Cellular Biochemistry, University of Kaiserslautern, Erwin-Schrödinger-Straße 13, D-67663 Kaiserslautern, Germany
[e] German Cancer Research Center (DKFZ), DKFZ-ZMBH Alliance, Im Neuenheimer Feld 280, D-69120 Heidelberg, Germany

ARTICLE INFO

Keywords:
Peroxiredoxin
Redox sensor
roGFP2
H_2O_2
Plasmodium falciparum

ABSTRACT

Redox-sensitive green fluorescent protein 2 (roGFP2) is a valuable tool for redox measurements in living cells. Here, we demonstrate that roGFP2 can also be used to gain mechanistic insights into redox catalysis *in vivo*. *In vitro* enzyme properties such as the rate-limiting reduction of wild type and mutant forms of the model peroxiredoxin *Pf*AOP are shown to correlate with the ratiometrically measured degree of oxidation of corresponding roGFP2 fusion proteins. Furthermore, stopped-flow kinetic measurements of the oxidative half-reaction of *Pf*AOP support the interpretation that changes in the roGFP2 signal can be used to map hyperoxidation-based inactivation of the attached peroxidase. Potential future applications of our system include the improvement of redox sensors, the estimation of absolute intracellular peroxide concentrations and the *in vivo* assessment of protein structure-function relationships that cannot easily be addressed with recombinant enzymes, for example, the effect of post-translational protein modifications on enzyme catalysis.

1. Introduction

Genetically encoded fusion constructs between redox enzymes and redox-sensitive fluorescent proteins are commonly used to make non-invasive redox measurements in living cells [1–4]. Fusion constructs between a peroxiredoxin (Prx), which serves as the peroxide sensor moiety, and redox-sensitive green fluorescent protein 2 (roGFP2), which serves as the reporter moiety, have recently been developed and allow real-time monitoring of intracellular hydroperoxide concentrations [4–6]. Here, we asked whether roGFP2 fusion constructs and hydroperoxide challenges can be used to deduce peroxidase properties and mechanisms *in vivo*. In other words, do classic enzyme kinetic parameters of peroxidases affect the roGFP2 readout in a predictable fashion? In particular, we were interested in understanding how roGFP2 readouts are affected by the peroxidase k_{cat}^{app} values and catalytic efficiencies (k_{cat}^{app}/K_m^{app} values reflecting second order rate constants) as well as inactivation kinetics due to hyperoxidation, *i.e.* the sulfinic and sulfonic acid formation of the active site cysteine residue.

To experimentally address these questions, we required a kinetically well-characterized peroxidase isoform and thus chose to use the Prx5-type model enzyme *Pf*AOP from the malaria parasite *Plasmodium falciparum*. *Pf*AOP localizes to the cytosol and plastid of the parasite, is dispensable for asexual blood stage development and accepts a variety of hydroperoxide substrates and electron donors *in vitro* [7–10]. Steady-state kinetics in combination with site-directed mutagenesis, X-ray structures and gel filtration analyses have previously revealed that *Pf*AOP requires only one cysteine residue for catalysis and predominantly forms stable homodimers [10,11]. This is in contrast to GPx3 and typical 2-Cys Prx [12,13], which have been used as ratiometric roGFP2-coupled peroxide sensors [3,5,6]. The latter peroxidases are either incompletely characterized regarding their kinetics or have more complicated reaction mechanisms due to the number of relevant cysteine residues and/or variable quaternary structures.

We have previously characterized the kinetic parameters of gain- and loss-of-function mutants of *Pf*AOP and showed that the enzyme is rapidly inactivated by H_2O_2 but not by *tert*-butyl hydroperoxide

* Corresponding authors.
** Corresponding author at: University of Kaiserslautern, Erwin-Schrödinger-Straße 54, D-67663 Kaiserslautern, Germany.
E-mail addresses: rradi@fmed.edu.uy (R. Radi), morgan@bio.uni-kl.de (B. Morgan), deponte@chemie.uni-kl.de (M. Deponte).
[1] These authors contributed equally to this work.

http://dx.doi.org/10.1016/j.redox.2017.10.017
Received 25 July 2017; Received in revised form 17 October 2017; Accepted 25 October 2017
Available online 26 October 2017

(*t*BOOH) [10,11]. Mutation of residue Leu^{109}, which is situated at the bottom of the active site between the catalytic (peroxidatic) cysteine residue Cys^{117} and the buried non-catalytic cysteine residue Cys^{143}, affects the catalytic as well as the inactivation properties of *Pf*AOP [11]. For example, compared to recombinant wild type *Pf*AOP, the gain-of-function mutant *Pf*AOP^{L109M} was shown to be less susceptible to H_2O_2-dependent inactivation and to have a 3-fold higher k_{cat}^{app} value for *t*BOOH, a 2.3-fold higher k_{cat}^{app} value for glutaredoxin (Grx) as an electron donor, and a 1.2- to 1.4-fold higher k_{cat}^{app} value for reduced glutathione (GSH) as an electron donor [11]. Furthermore, the k_{cat}^{app}/K_m^{app} values of *Pf*AOP^{L109M} for Grx and GSH increased 2.2- and 12-fold, respectively, whereas the k_{cat}^{app}/K_m^{app} value for tBOOH was similar to the wild type enzyme. In contrast, the loss-of-function mutant *Pf*AOP^{L109A} was shown to be more susceptible to H_2O_2-dependent inactivation, to have 4-fold lower k_{cat}^{app} values for *t*BOOH and GSH, a 7-fold lower k_{cat}^{app}/K_m^{app} value for tBOOH and a 3-fold lower k_{cat}^{app}/K_m^{app} value for GSH. The activating effects for *Pf*AOP^{L109M} depended on the presence of residue Cys^{143}, although its exact role could not be resolved by steady-state kinetics or gel mobility shift assays. Based on our kinetic and structural data, we proposed a model according to which Leu^{109} and Cys^{143} together affect the equilibrium between the fully folded and locally unfolded conformation of *Pf*AOP. Mutation of Leu^{109} to methionine was suggested to stimulate local unfolding of the active site helix α2, thereby preventing hyperoxidation and promoting the probably rate-limiting GSH-dependent reduction of the Cys^{117} sulfenic acid [11]. Here we used our gain- and loss-of-function mutants to compare the oxidative half-reaction using stopped-flow kinetics and to test the suitability of roGFP2 as a mechanistic reporter for redox catalysis inside living cells.

2. Materials and methods

2.1. Materials

H_2O_2, *t*BOOH, peroxynitrite, cumene hydroperoxide and 12(S)-hydroperoxy-5Z,8Z,10E,14Z eicosatetraenoic acid (12(S)HpETE) were purchased from Mallinckrodt Chemicals or Sigma. The concentration of H_2O_2 stock solutions was determined spectrophotometrically at 240 nm ($\varepsilon_{240\ nm}$ = 43.6 M^{-1} cm^{-1}). The peroxynitrite concentration was determined at alkaline pH at 302 nm ($\varepsilon_{302\ nm}$ = 1.67 mM^{-1} cm^{-1}) [14]. Concentrations of cumene hydroperoxide and 12(S)HpETE were calculated considering the manufactures specifications. Diamide, 1,4-dithiothreitol (DTT), diethylenetriaminepentaacetic acid (DTPA) and horseradish peroxidase were purchased from Sigma. Nickel-nitrilotriacetic acid agarose (Ni-NTA) was from Qiagen. HiTrap desalting columns were from Amersham Bioscience. All of the amino acids, glucose and yeast nitrogen base required for Hartwell's Complete (HC) yeast growth medium were purchased from Sigma. Flat-bottom 96 well microplates (product #353219) were from BD Biosciences.

2.2. Cloning of yeast expression vectors

The gene sequence for N-terminally truncated *Pf*AOP$^{\Delta 59}$ without its apicoplast-targeting sequence [7,10] (herein after referred to as *Pf*AOP) was optimized for expression in *Saccharomyces cerevisiae*, synthesized and cloned into a pUC57 vector (Genscript, Piscataway, USA). *PfAOP* was subcloned into *roGFP2-GRX1*/p416TEF [15] using *Eco*RI and *Hin*dIII restriction sites, thereby replacing *GRX1* to generate wild type *roGFP2-PFAOP^{wt}*/p416TEF. A standard site-directed mutagenesis protocol was employed to generate *roGFP2-PFAOP^{L109M}*/p416TEF, *roGFP2-PFAOP^{L109A}*/p416TEF and *roGFP2-PFAOP^{C143S}*/p416TEF. All mutations were confirmed by Sanger sequencing. The codon-optimized gene sequence encoding roGFP2-*Pf*AOP has been deposited in GenBank (http://www.ncbi.nlm.nih.gov/genbank/) under accession number MF140392 and is listed in the Supplementary material.

2.3. Transformation, expression and fluorescence measurements in S. cerevisiae

Plasmids p416TEF, *roGFP2*/p416TEF and wild type and mutant forms of *roGFP2-PFAOP*/p416TEF were transformed into yeast strain BY4742 and roGFP2 measurements were conducted as described previously [3,4]. Briefly, liquid cultures were grown to late exponential phase (OD_{600} = 3–4) in HC medium lacking uracil, in order to select for those cells retaining the p416TEF vectors. Cells were harvested by centrifugation for 3 min at 800 × *g* and resuspended in buffer containing 100 mM NaCl, 100 mM sorbitol, 100 mM Tris-HCl, pH 7.4 to a final concentration of 7.5 OD_{600} units/mL. Aliquots of 200 µL of the cell suspension were transferred into the appropriate number of wells of a flat-bottom 96 well microplate. Two additional wells were utilized for controls and were supplemented with either diamide to a final concentration of 20 mM (fully oxidized control) or DTT to a final concentration of 100 mM (fully reduced control). The control wells are required for the determination of the degree of sensor oxidation (OxD). Cells in the experimental wells were treated with twelve increasing concentrations of H_2O_2 or *t*BOOH (10–500 µM) and responses were followed for up to 100 min at 30 °C using a CLARIOstar fluorescence plate reader (BMG Labtech). For each peroxide concentration the OxD was plotted against time. The area under the curve (AUC (OxD × min)) was subsequently calculated in Excel and plotted against the according peroxide concentration in SigmaPlot 13. All data were averaged from triplicate (*t*BOOH treatment) or quadruplicate (H_2O_2 treatment) measurements from independent yeast cultures. Statistical analyses were carried out in SigmaPlot 13 using the One-way ANOVA method.

2.4. Expression and purification of recombinant wild type and mutant PfAOP in Escherichia coli

Recombinant proteins were expressed and purified by affinity-chromatography as described previously [10,11,16]. Briefly, *E. coli* XL1-Blue cells were transformed with plasmid *PFAOP*/pQE30, *PFAOP^{C117S}*/pQE30, *PFAOP^{C143S}*/pQE30 or *PFAOP^{L109M}*/pQE30. Expression was induced with 0.5 mM isopropyl-β-D-1-thiogalactopyranoside for 4 h at 37 °C. Liquid cultures were harvested by centrifugation for 15 min at 4000 × *g* and 4 °C. The bacteria were resuspended in buffer containing 20 mM imidazole, 300 mM NaCl, 50 mM $Na_xH_yPO_4$, pH 8.0, incubated with lysozyme and disrupted by sonication. Proteins were affinity-purified on Ni-NTA agarose columns and eluted in buffer containing 200 mM imidazol, 300 mM NaCl, 50 mM $Na_xH_yPO_4$, pH 8.0. Subsequently, samples were treated with 5 mM DTT for 30 min at 4 °C to fully reduce the protein. Remaining imidazole and DTT were removed using HiTrap desalting columns that were equilibrated with buffer containing 100 mM $Na_xH_yPO_4$, 0.1 mM DTPA, pH 7.4. Protein elution was monitored at 280 nm using an Äkta FPLC system. The protein concentration was determined spectrophotometrically using the molar extinction coefficient $\varepsilon_{280\ nm}$ = 21.43 mM^{-1} cm^{-1} as calculated for the primary sequence of the protein using the ProtParam ExPASy tool (http://web.expasy.org/protparam/). The thiol content of the proteins was analyzed with 5,5′-dithiobis-(2-nitrobenzoic acid) [17] revealing that 97% of the protein thiols were in a reduced state (data not shown).

2.5. Stopped-flow peroxidase measurements of recombinant wild type and mutant PfAOP

The oxidative half-reaction of 1 µM wild type *Pf*AOP, *Pf*AOP^{C117S}, *Pf*AOP^{C143S}, and *Pf*AOP^{L109M} with different hydroperoxides and peroxynitrite was analyzed using a SX-20 stopped-flow spectrofluorometer (Applied Photophysics). All activities were determined at 25 °C in 100 mM $Na_xH_yPO_4$ buffer containing 0.1 mM DTPA, pH 7.4. *Pf*AOP^{C117S} showed no change in fluorescence and served as a negative control. Two alternative methods were employed:

A) Direct assay: Changes of the intrinsic tryptophan fluorescence (λ_{exc} = 295 nm, total emission) of reduced wild type and mutant *Pf*AOP were followed after mixing of the enzymes with 1–100 µM H_2O_2, peroxynitrite, cumene hydroperoxide or 12(S)HpETE. Experimental curves showed two main phases of fluorescence change, which were fitted to exponential curves using the Applied Photophysics Pro-data SX software. The first phase, which was recorded from 2 ms (mixing time of the apparatus) to 20–100 ms depending on the peroxide concentration, showed a decrease in fluorescence. The second phase was followed from 0.1 to 10 s and showed a slower increase in fluorescence. After 10 s there was a further small increase in fluorescence, particularly at higher peroxide concentrations, which was disregarded for the fitting. Rate constants k_{obs} for the first and the second phase of fluorescence change were obtained from the exponential curves by analyzing the average of 5–6 runs. Rate constants $k_{1\text{-}3}$ were calculated from linear fits by plotting the obtained k_{obs} values against the peroxide concentrations [18–20]. Constants k_1 and k_2 were obtained from the slope of the first and the second plot, respectively. Rate constant k_3 was obtained from the y-axis intercept of the second plot. Alternative global fitting approaches did not yield better results and complicated the data interpretation because of even more unknown variables and unexplained rate constants.

B) Competition assay: The rate constant for the reaction between the enzymes and H_2O_2 or peroxynitrite (k_1*) was determined in a competition assay using horseradish peroxidase (HRP) as an alternative peroxide target as described previously [21,22]. Briefly, the oxidation of 2 µM HRP by 1 µM peroxide to 'compound I′ was followed at 398 nm ($\varepsilon_{398\ nm}$ = 42 $mM^{-1}\ cm^{-1}$) [23] in the absence or presence of increasing *Pf*AOP concentrations. The determined rate constant for the reaction of HRP with H_2O_2 and peroxynitrite was 1.4 × $10^7\ M^{-1}\ s^{-1}$ and 3.5 × $10^6\ M^{-1}\ s^{-1}$, respectively, in agreement with the previously reported values [22,24]. The rate constants for the reactions of wild type and mutant *Pf*AOP with the peroxide were calculated from the amount of compound I that was formed at different *Pf*AOP concentrations.

3. Results

3.1. The gain-of-function mutant $PfAOP^{L109M}$ serves as a robust hydroperoxide sensor in yeast

Baker's yeast *Saccharomyces cerevisiae* is a well-established model organism for studying roGFP2-dependent redox sensing [3,6]. Therefore, we chose to use it for the exemplary intracellular assessment of the catalytic mechanism and inactivation properties of *Pf*AOP. First, we cloned codon-optimized fusion constructs encoding wild type roGFP2-*Pf*AOP (Genbank accession number MF140392 and Supplementary material) as well as different variants containing *Pf*AOP with Leu^{109} or Cys^{143} mutations into the vector p416TEF.

The p416TEF plasmids were transformed into wild type BY4742 yeast cells for cytosolic expression of the constructs. The yeast cells were subsequently treated with 10–500 µM H_2O_2 and the ratiometric degree of roGFP2 oxidation (OxD) was monitored over time. Striking differences were observed between the wild type roGFP2-*Pf*AOP fusion construct (wt) and the L109M mutant (Fig. 1a,b). As a first readout parameter we assessed the maximum change in roGFP2 oxidation (ΔOxD_{max}). ΔOxD_{max} for L109M was higher than for the wild type fusion construct at most H_2O_2 concentrations. At H_2O_2 concentrations above 200 µM, the response of the wt construct decreased sharply, whilst, in contrast, the response of L109M was more robust. Comparable OxD responses were obtained following *t*BOOH treatment, although no decrease of ΔOxD_{max} was observed at higher *t*BOOH concentrations (Fig. 1c,d). In summary, $PfAOP^{L109M}$ is not only more active and robust than wild type *Pf*AOP *in vitro* but its catalytic and inactivation properties with H_2O_2 and *t*BOOH are also reflected by the

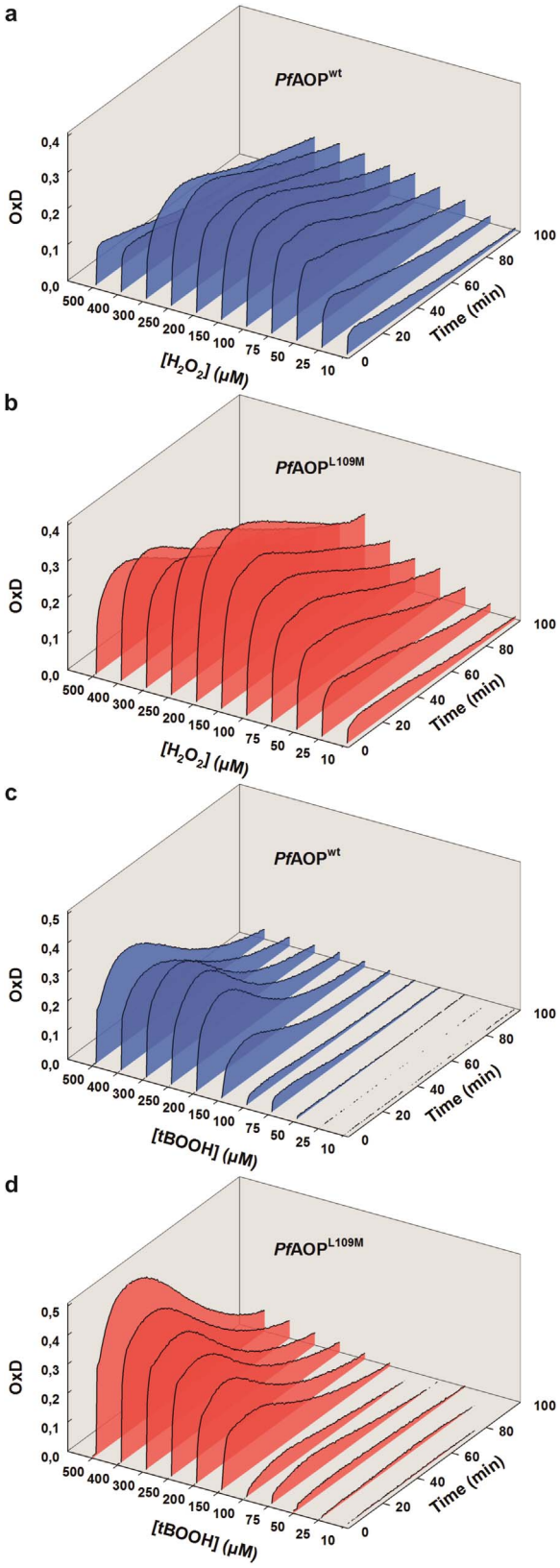

Fig. 1. Dose-response curves for yeast cells with genetically encoded roGFP2-*Pf*AOP fusion constructs after bolus treatments with hydroperoxides at 30 °C. (A) Time-course measurements of the ratiometric degree of oxidation (OxD) for the wild type roGFP2-*Pf*AOP fusion construct (wt) at different initial H_2O_2 concentrations. (B) Time-course measurements of the OxD for the roGFP2-$PfAOP^{L109M}$ fusion construct (L109M) at different initial H_2O_2 concentrations. (C) and (D) Time-course measurements of the OxD for wt and L109M at different initial *t*BOOH concentrations. Data were averaged from four (H_2O_2) or three (*t*BOOH) independent biological replicates.

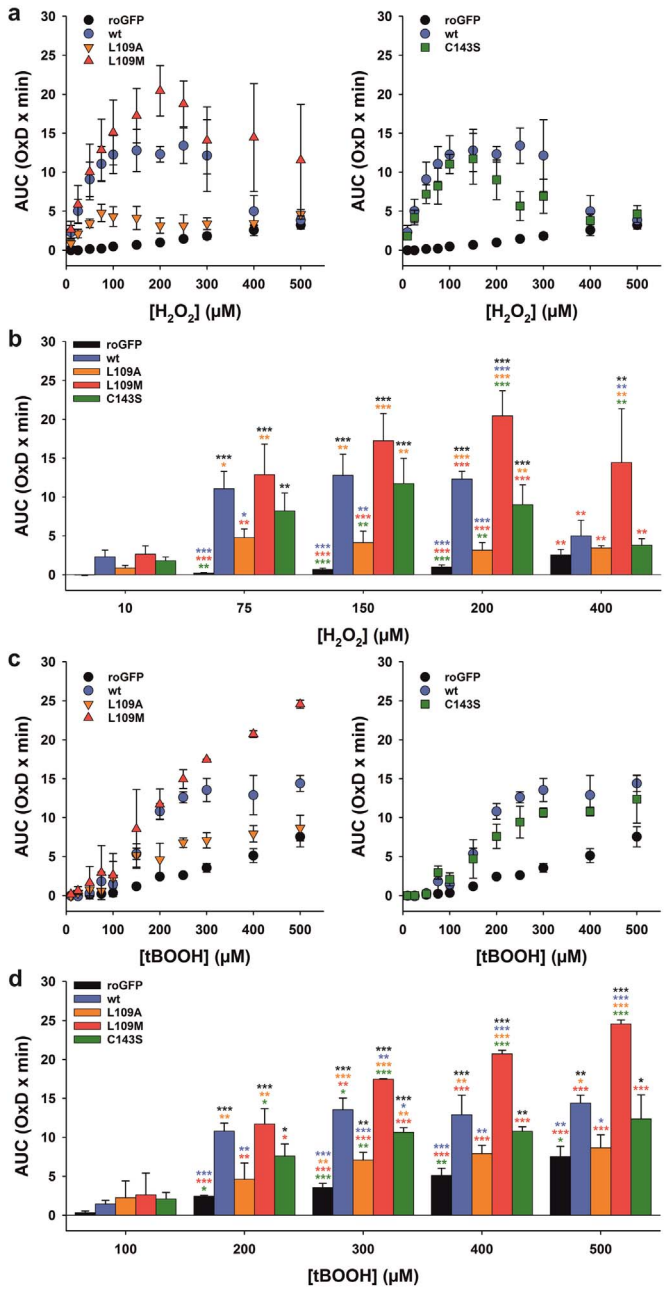

Fig. 2. Integrated dose-response curves for yeast cells with genetically encoded roGFP2-*Pf*AOP fusion constructs after bolus treatments with hydroperoxides. Wild type roGFP2-*Pf*AOP (wt) and roGFP2 alone (roGFP) served as positive and negative control, respectively, and confirmed that the OxD was *Pf*AOP-dependent. Constructs roGFP2-*Pf*AOP^{L109A} (L109A), roGFP2-*Pf*AOP^{L109M} (L109M) and roGFP2-*Pf*AOP^{C143S} (C143S) carry previously characterized single point mutations of *Pf*AOP [11]. (A) The area under the OxD curves (AUC) from Fig. 1 was determined between 0–60 min and plotted against the initial H_2O_2 concentration. All data were averaged from quadruplicate independent biological replicates. (B) Statistical analysis of the data from panel a. P-values were calculated using the One-way ANOVA method in SigmaPlot 13. (C) AUC from Fig. 1 plotted against the initial *t*BOOH concentration. All data were averaged from triplicate independent biological replicates. (D) Statistical analysis of the data from panel c. *$p < 0.05$; **$p < 0.01$; ***$p < 0.001$.

different roGFP2 responses of the L109M and wt fusion constructs in yeast cells.

3.2. Intracellular comparison of PfAOP mutants and quantification of roGFP2 readouts

In order to enable a more statistically rigorous comparison between different constructs, we integrated the area below the OxD curve, henceforth referred to as Area Under Curve (AUC), including the mutants L109A and C143S (Fig. 2a). In contrast to L109M, the L109A construct exhibited a decreased AUC, relative to the wt construct, for all H_2O_2 concentrations tested. Replacement of the non-catalytic second cysteine residue of *Pf*AOP in C143S also slightly decreased the AUC compared to the wt construct at some H_2O_2 concentrations. Most of the differences among the wild type and mutant *Pf*AOP fusion constructs were statistically significant with $p < 0.01$ (Fig. 2b). Similar differences between the AUCs of wt, L109M, L109A and C143S were also observed for roGFP2 responses to challenges with *t*BOOH (Fig. 2c,d).

As a third readout parameter we analyzed the H_2O_2 concentration-dependence of the AUC. The H_2O_2 concentration at which the highest AUC was observed (cH_2O_{2max}) was noticeably lower for the L109A construct compared to the wt and L109M constructs (Fig. 2a,b). Furthermore, a decrease in AUC was observed for the L109A and wt constructs at H_2O_2 concentrations above 75 μM and 250 μM, respectively. At 400 and 500 μM H_2O_2 the AUC of these constructs was not significantly different to the roGFP2 negative control. In contrast, the AUC of the L109M construct indicated robust roGFP2 responses even at the highest H_2O_2 concentrations tested. Following treatment with *t*BOOH, the AUC was observed to either show an increase at all tested concentrations (L109M) or to reach a plateau only at much higher *t*BOOH concentrations relative to H_2O_2 (wt, L109A and C143S) (Fig. 2c,d). Please note that the AUC of the roGFP2 negative control increased with increasing *t*BOOH concentrations. Thus, the observed AUC plateau for wt, L109A and C143S at 300–500 μM *t*BOOH rather indicates a decrease of the peroxidase-dependent roGFP2 response of these constructs. In summary, enzymatic properties of gain- and loss-of-function mutants of *Pf*AOP as determined *in vitro* correlate with changes in ΔOxD_{max}, the AUC and the cH_2O_{2max} of roGFP2 fusion constructs in yeast cells. Differences between mutants can be quantified and statistically analyzed using AUC values and allow us to monitor mechanistic aspects of peroxiredoxin catalysis in real-time in living cells.

3.3. In vitro oxidation and hyperoxidation kinetics of PfAOP

As outlined above, the role of residues Leu^{109} and Cys^{143} for H_2O_2-dependent *Pf*AOP catalysis and hyperoxidation-dependent enzyme inactivation could not be resolved by steady-state kinetics or gel mobility shift assays [11]. In order to address a potential relevance of the oxidative half-reaction and/or the hyperoxidation of *Pf*AOP for intracellular roGFP2 readouts, we performed stopped-flow kinetic experiments with recombinant *Pf*AOP^{wt}, *Pf*AOP^{C143S} and *Pf*AOP^{L109M}. The reaction between reduced *Pf*AOP and H_2O_2 was directly monitored at variable peroxide concentrations by following changes in the intrinsic tryptophan fluorescence of the enzyme (Fig. 3). Two major phases were detected, one rapid decrease followed by a slower increase in fluorescence. Three rate constants were assigned to the reaction kinetics (Fig. S1), one [H_2O_2]-dependent rate constant for the first phase (k_1) and one [H_2O_2]-dependent as well as one [H_2O_2]-independent rate constant for the second phase (k_2 and k_3, respectively). *Pf*AOP^{wt} and *Pf*AOP^{C143S} had similar kinetics with a second-order rate constant k_1 of ~3.5 × 10^7 M^{-1} s^{-1} (Fig. 3a,b and Table 1). A spectrophotometric competition assay with horseradish peroxidase revealed a rate constant k_1* of 2.1 × 10^7 M^{-1} s^{-1} and confirmed that k_1 reflects the reaction between *Pf*AOP and the peroxide (Fig. S2 and Table 1). The peroxidase competition assay also showed that the rate constant k_1 for the sulfenic acid formation of *Pf*AOP^{L109M} is identical to *Pf*AOP^{wt} and *Pf*AOP^{C143S}. However, the rate constant k_2 of *Pf*AOP^{L109M} at around 1.4 × 10^3 M^{-1} s^{-1} was more than one order of magnitude smaller than for *Pf*AOP^{wt} and *Pf*AOP^{C143S}. The smaller k_2 value probably indicates a slower rate of hyperoxidation owing to reaction with a second molecule of H_2O_2 (see also Section 4). The relevance of rate constant k_3 is unclear. Maybe it reflects a slow conformational change. Please note that we observed only a small change in fluorescence for *Pf*AOP^{L109M} compared to *Pf*AOP^{wt} (Fig. 3a,c),

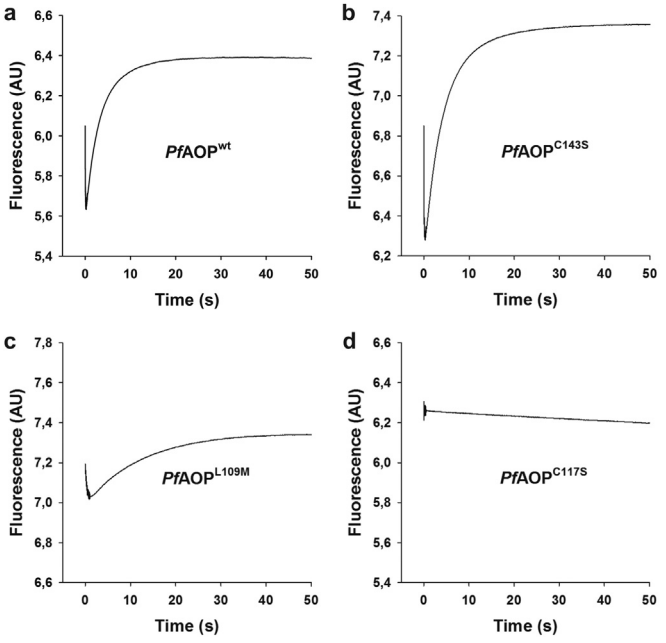

Fig. 3. Stopped-flow kinetics of the oxidative half-reaction of reduced recombinant *Pf*AOP after mixing with H_2O_2 at pH 7.4 and 25 °C. Representative traces are shown for 1 μM enzyme and 1 μM substrate. (A) Kinetics for wild type *Pf*AOP. (B) Kinetics for *Pf*AOP^{C143S} lacking the non-catalytic second cysteine residue. (C) Kinetics for the active site mutant *Pf*AOP^{L109M}. (D) *Pf*AOP^{C117S} without the peroxidatic cysteine residue served as a negative control.

which might be explained if only a fraction of *Pf*AOP^{L109M} adopted the fully folded conformation (see also Discussion). Although this indicates a lower availability of the enzyme for the reaction with H_2O_2, this has no effect on the second order rate constants k_1. Control experiments with *Pf*AOP^{C117S} revealed that all rate constants and phases depended on the presence of the peroxidatic cysteine of the enzyme (Fig. 3d).

Next, we tested the peroxide-dependence of the oxidative half-reaction using H_2O_2, peroxynitrite, cumene hydroperoxide, and the fatty acid hydroperoxide 12(S)HpETE (Table 2). Rate constant k_1 of *Pf*AOP^{wt} was similar for all peroxide substrates tested except for aromatic cumene hydroperoxide, which was converted three- to sevenfold slower. Rate constants k_2 and k_3 did not appear to depend on the type of peroxide. In summary, stopped-flow kinetic measurements of the oxidative half-reaction showed that the reactivities of reduced *Pf*AOP^{wt}, *Pf*AOP^{C143S} and *Pf*AOP^{L109M} with H_2O_2 are very similar. *Pf*AOP^{L109M} differs from the other enzymes with regard to rate constant k_2, which might reflect the hyperoxidation kinetics. Furthermore, reactivities of *Pf*AOP^{wt} with H_2O_2, peroxynitrite, and 12(S)HpETE are very similar, suggesting that there is no real enzyme-substrate complex and that the reaction proceeds as soon as the substrate enters the active site in a productive orientation.

4. Discussion

How can we integrate and interpret the roGFP2 readouts and stopped-flow kinetic data with previous kinetic data in a comprehensive model? The ΔOxD_{max} and AUC values probably represent a metabolic flux comprising (i) the peroxide-dependent oxidation of the sensor moiety (yielding a Prx sulfenic acid species), (ii) the two-step reduction of the sensor by the reporter moiety (yielding a roGFP2 disulfide), and (iii) the reduction of the reporter moiety by GSH, Grx or another cytosolic thiol component (Fig. 4). Furthermore, there are side reactions that prevent the oxidation of the reporter moiety, including (iv) the potential reduction of the sulfenic acid by other thiols than the reporter moiety, and (v) the hyperoxidation of the sensor moiety. The stopped-flow kinetic data indicate that rate constant k_1 reflects the sulfenic acid formation and that this constant is similar for *Pf*AOP^{wt}, *Pf*AOP^{L109M}, and *Pf*AOP^{C143S}. Furthermore, rate constant k_1 is very similar for different peroxides (except for aromatic cumene hydroperoxide). Thus, step (i) did probably not account for the observed differences for wild type and mutant *Pf*AOP fusion constructs after treatment with H_2O_2 and *t*BOOH. Similar k_1 values of the oxidative half-reaction might in fact explain the similar sensitivity of the roGFP2 constructs in terms of the lowest detectable peroxide concentration. Step (iii) probably also did not account for the observed differences between the roGFP2 readouts, because the roGFP2 reporter moiety and the genetic background were identical for all analyzed constructs. Step (iv) includes several unknown variables, but the fact that the roGFP2-*Pf*AOP fusion constructs were quite sensitive and responded well to peroxide challenges suggests that this bypass reaction was presumably not a major factor for the roGFP2 readouts.

The crucial remaining parameters in Fig. 4 are step (ii) and/or step (v). A rate-limiting sensor reduction by roGFP2, which is promoted in L109M and hampered in L109A, is in excellent agreement with our previous *in vitro* studies. In particular, the AUCs of L109M > wt >

Table 1
Rate constants for the oxidative half-reaction of 1 μM reduced recombinant wild type and mutated forms of *Pf*AOP as determined by stopped-flow kinetic measurements with variable H_2O_2 concentrations at pH 7.4 and 25 °C.

	k_1*[a] (M^{-1} s^{-1})	k_1 (M^{-1} s^{-1})	k_2 (M^{-1} s^{-1})	k_3 (s^{-1})
PfAOP^{wt}	(2.1 ± 0.8) × 10^7	(3.2 ± 0.5) × 10^7	(3.6 ± 0.6) × 10^4	0.28 ± 0.02
PfAOP^{C143S}	(2.2 ± 0.6) × 10^7	(3.7 ± 1.5) × 10^7	(4.3 ± 0.0) × 10^4	0.16 ± 0.01
PfAOP^{L109M}	(2.0 ± 0.8) × 10^7	n.d.	(1.4 ± 0.1) × 10^3	0.04 ± 0.00

n.d.: not determined.
[a] Rate constant k_1* was determined in a peroxidase competition assay.

Table 2
Rate constants for the oxidative half-reaction of 1 μM reduced recombinant wild type *Pf*AOP as determined by stopped-flow kinetic measurements with variable peroxide concentrations at pH 7.4 and 25 °C.

	k_1*[a] ($M^{-1}s^{-1}$)	k_1 ($M^{-1}s^{-1}$)	k_2 ($M^{-1}s^{-1}$)	k_3 (s^{-1})
Peroxynitrite	(2.6 ± 1.9) × 10^7	(1.5 ± 0.5) × 10^7	n.d.	n.d.
Hydrogen peroxide	(2.1 ± 0.8) × 10^7	(3.2 ± 0.5) × 10^7	(3.6 ± 0.6) × 10^4	0.28 ± 0.02
Cumene hydroperoxide	n.d.	(4.8 ± 0.5) × 10^6	(4.5 ± 2.7) × 10^4	0.27 ± 0.17
12(S)HpETE	n.d.	(1.9 ± 0.6) × 10^7	(5.6 ± 1.2) × 10^4	0.45 ± 0.05

n.d.: not determined.
[a] Rate constant k_1* was determined in a peroxidase competition assay.

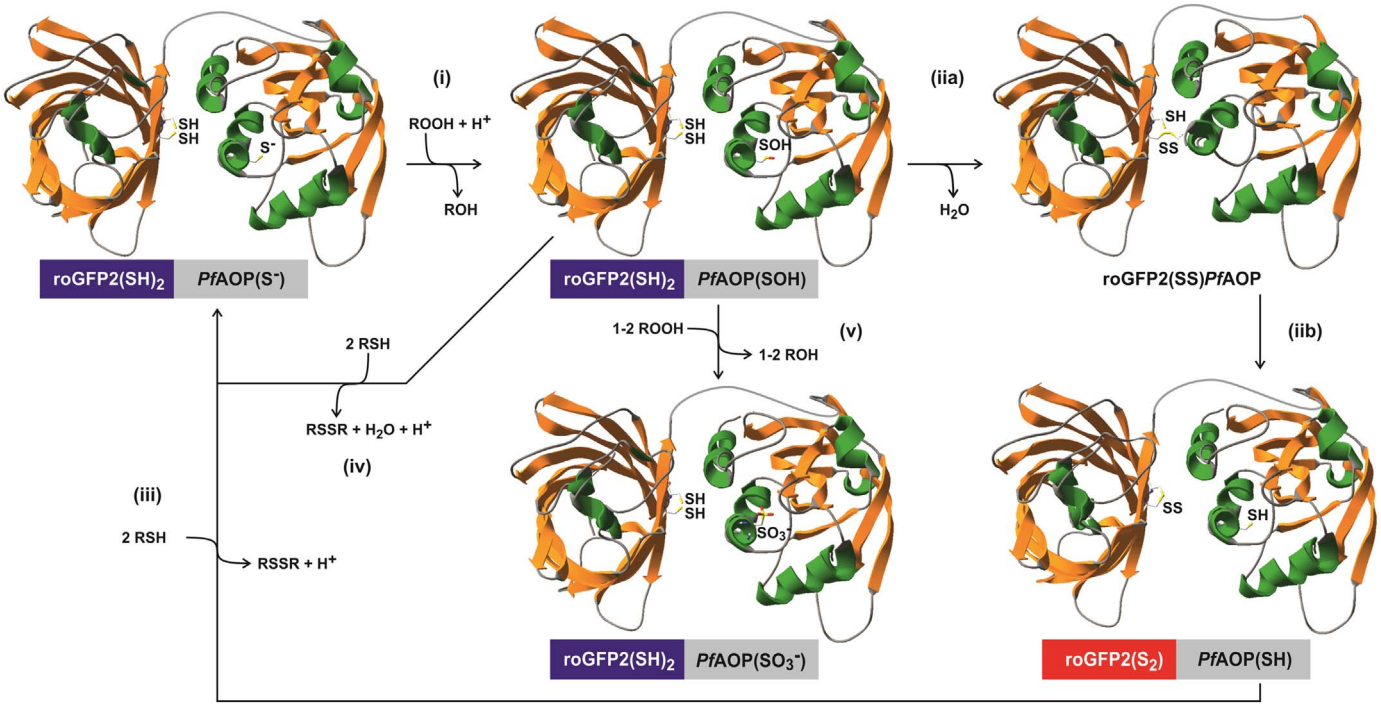

Fig. 4. Model for the intracellular roGFP2-dependent assessment of *Pf*AOP catalysis. The metabolic flux monitored by roGFP2 comprises (i) the peroxide-dependent oxidation of the *Pf*AOP sensor moiety, (ii) the two-step reduction of the sensor moiety yielding the oxidized roGFP2 reporter moiety, (iii) the reduction of the reporter moiety, (iv) a potential roGFP2-independent bypass reaction between oxidized *Pf*AOP and alternative reducing agents, and (v) the inactivation of the sensor moiety because of hyperoxidation.

L109A correlate well with the corresponding k_{cat}^{app} values of the rate-limiting reductive half-reaction with GSH *in vitro* [11]. Although step (ii) reflects the electron transfer between reduced roGFP2 and the sulfenic acid of *Pf*AOP instead of the transfer between GSH and *Pf*AOP, both processes should depend in a similar way on the Leu^{109}-dependent local unfolding of the active site helix α2 (step iia). A correlation between the enzyme activity and the AUC is also supported for recombinant $PfAOP^{C143S}$, which was shown to have a 25% lower activity *in vitro* [10], in accordance with the apparently slightly decreased roGFP2 response of C143S in yeast. Step (v), the hyperoxidation of the peroxidatic cysteine, inactivates the sensor and prevents the oxidation of the roGFP2 reporter moiety. Thus, Prx inactivation by hyperoxidation is probably the most crucial factor affecting cH_2O_{2max} and the decrease in AUC at higher H_2O_2 concentrations. Recombinant wild type *Pf*AOP was shown to be rapidly inactivated by H_2O_2, whereas inactivation by *t*BOOH required much higher peroxide concentrations *in vitro* [11]. These findings correlate with the observation that the highest AUC of the wt construct was reached at much higher *t*BOOH concentrations compared to H_2O_2. Furthermore, recombinant $PfAOP^{L109A}$ and $PfAOP^{L109M}$ were more and less susceptible to H_2O_2-dependent inactivation, respectively [11], which correlates with the robustness of the roGFP2 responses of the L109A and L109M constructs. The more than ten times smaller rate constant k_2 of recombinant $PfAOP^{L109M}$ determined by stopped-flow measurements also supports a slower enzyme inactivation in accordance with the increased robustness of the L109M construct in yeast. Again, the data is consistent with a catalytic model that suggests a slower hyperoxidation due to the shifted equilibrium towards the locally unfolded conformation for $PfAOP^{L109M}$ [11]. Overall, we observed a strong correlation between the sensitivity of the different roGFP2-*Pf*AOP constructs to hyperoxidation with H_2O_2 in contrast to *t*BOOH and the known inactivation properties of recombinant *Pf*AOP mutants *in vitro*. Importantly, the roGFP2 fusion constructs allow us to analyze the intracellular H_2O_2 responses of wild type and mutant *Pf*AOP *in vivo*, whereas *in vitro* NADPH-coupled steady-state kinetic measurements require H_2O_2 concentrations ≥ 5 μM, which result in rapid enzyme inactivation and hamper in-depth analysis [11].

In summary, ratiometric roGFP2 measurements of Prx-fusion constructs in combination with site-directed mutagenesis are a powerful tool to gather mechanistic insights on Prx catalysis and inactivation *in vivo*.

What are the implications of our study? (i) The identification of correlations between roGFP2 readouts and kinetic parameters as well as inactivation properties of Prx might be useful for the optimization of redox sensors, *e.g.,* by searching the literature for peroxidases that have highly efficient reductive half-reactions and that are not prone to inactivation (*e.g.,* selected bacterial Prx-isoforms) [25]. (ii) Peroxidase fusion constructs with roGFP2 could be also useful for addressing inactivation properties that cannot be analyzed in steady-state kinetic assays, as shown for the reaction between H_2O_2 and wild type or mutant *Pf*AOP [11]. Interesting candidates might be, for example, the Prx6-type 1-Cys peroxiredoxins [26,27], which are almost inactive in standard assays (maybe owing to rapid inactivation) and remain to be analyzed in much more detail. Potential limitations of the method include genetic manipulations to remove much more active competing peroxidases in order to increase the OxD and AUC responses. (iii) Recombinant proteins often lack post-translational modifications (*e.g.,* when purified from *E. coli*) or are obtained in rather low yields (*e.g.,* when purified from insect cells). The analysis of roGFP2-coupled wild type and mutant enzymes might allow the *in vivo* evaluation of the relevance of post-translational modifications for Prx catalysis [28]. For example, serine/threonine to alanine/valine or glutamate mutants could be compared in order to directly monitor the role of phosphorylation sites, *e.g.,* at the plasma membrane or the centrosome [29–33]. Potential limitations of the method comprise genetic manipulations to prevent the formation of heterooligomers with endogenous Prx copies as well as altered quaternary structures because of the bulky roGFP2-tag. (iv) Absolute values for the cytosolic H_2O_2 concentration in yeast and the diffusion-dependent ratio between extra- and intracellular H_2O_2 are, to the best of our knowledge, unknown. The latter ratio is of particular importance to judge the physiological relevance of bolus treatments with H_2O_2. Estimated steady-state and physiological peak concentrations for H_2O_2 in a variety of organisms are ~1 nM and 0.5–0.7 μM, respectively [34]. Based on the observation that the

activity of recombinant *Pf*AOP^{L109M} peaked in steady-state kinetic measurements at 10 μM [11], we speculate that the intracellular H_2O_2 concentration in our experiments might have been roughly 20-fold lower than the extracellular H_2O_2 concentration because of the ΔOxD_{max} concentration for H_2O_2 in Fig. 1b at 200 μM. Although the yeast plasma membrane permeability for H_2O_2 was shown to be variable [35,36], a 20-fold difference in H_2O_2 concentration across the plasma membrane is in good agreement with reports on 7- to 10-fold decreased intracellular H_2O_2 concentrations upon bolus treatments of *E. coli* or mammalian cells [37–39]. Hence, assuming a linear correlation between the extra- and intracellular H_2O_2 concentration, intracellular H_2O_2 concentrations in our experiments might have ranged from 0.5 to 25 μM. Thus, using the inactivation properties of *Pf*AOP^{L109M} for an estimation of the intracellular H_2O_2 concentration, we speculate that common bolus treatments in yeast research might result in intracellular H_2O_2 concentrations that significantly exceed a physiological threshold concentration around 0.7 μM [34].

5. Conclusions

Fusion constructs between roGFP2 and Prx have been commonly used to monitor intracellular hydroperoxide concentrations, but, so far, it was unknown how and to which extent kinetic parameters or inactivation properties of the Prx sensor are correlated with the measured roGFP2 readout. Here we showed for fusion constructs between roGFP2 and gain- and loss-of-function mutants of the model peroxiredoxin *Pf*AOP that *in vitro* k_{cat}^{app} values and inactivation properties of Prx correlate with the roGFP2 readout inside living cells. The findings of our proof-of-principle study open the door to a wide-range of potential future applications, including (i) the optimization of redox sensors, (ii) the noninvasive analysis of peroxidases, in particular, of enzymes that are labile or prone to inactivation *in vitro*, (iii) the evaluation of the relevance of post-translational protein modifications, and (iv) the estimation of absolute intracellular hydroperoxide concentrations.

Acknowledgments

This work was supported by the priority program SPP 1710 of the Deutsche Forschungsgemeinschaft (grants DE 1431/8-1 and DE 1431/8-2 to M.D., grant DI 731/3-2 to T.P.D. and grant MO 2774/2-1 to B.M.) and grants from Universidad de la República, Uruguay (CSIC Grupos 767, CSIC I + D 2016 367 and Espacio Interdisciplinario). The position of M.D. was funded by the Deutsche Forschungsgemeinschaft in the frame of the Heisenberg programme (Grant DE 1431/9-1). The authors declare no competing financial interests.

Author contributions

V.S. and T.D. performed the roGFP2 experiments with the support of B.M. and T.P.D. V.S. and M.T. performed the stopped-flow experiments. B.M. conceived and supervised the roGFP2 experiments. M.T. and R.R. conceived and supervised the stopped-flow experiments. V.S., B.M. and M.D. analyzed the roGFP2 data. V.S., M.T. and R.R. analyzed the stopped-flow data. M.D. conceived and supervised the study and M.D. and B.M. wrote the manuscript. All authors discussed the results and gave approval to the final version of the manuscript.

Appendix A. Supplementary material

Supplementary data associated with this article can be found in the online version at http://dx.doi.org/10.1016/j.redox.2017.10.017.

References

[1] V.V. Belousov, A.F. Fradkov, K.A. Lukyanov, D.B. Staroverov, K.S. Shakhbazov, A.V. Terskikh, S. Lukyanov, Genetically encoded fluorescent indicator for intracellular hydrogen peroxide, Nat. Methods 3 (4) (2006) 281–286.
[2] M. Gutscher, A.L. Pauleau, L. Marty, T. Brach, G.H. Wabnitz, Y. Samstag, A.J. Meyer, T.P. Dick, Real-time imaging of the intracellular glutathione redox potential, Nat. Methods 5 (6) (2008) 553–559.
[3] B. Morgan, M.C. Sobotta, T.P. Dick, Measuring E(GSH) and H2O2 with roGFP2-based redox probes, Free Radic. Biol. Med. 51 (11) (2011) 1943–1951.
[4] M. Schwarzlander, T.P. Dick, A.J. Meyer, B. Morgan, Dissecting redox biology using fluorescent protein sensors, Antioxid. Redox Signal 24 (13) (2016) 680–712.
[5] M. Gutscher, M.C. Sobotta, G.H. Wabnitz, S. Ballikaya, A.J. Meyer, Y. Samstag, T.P. Dick, Proximity-based protein thiol oxidation by H2O2-scavenging peroxidases, J. Biol. Chem. 284 (46) (2009) 31532–31540.
[6] B. Morgan, K. Van Laer, T.N. Owusu, D. Ezerina, D. Pastor-Flores, P.S. Amponsah, A. Tursch, T.P. Dick, Real-time monitoring of basal H2O2 levels with peroxiredoxin-based probes, Nat. Chem. Biol. 12 (6) (2016) 437–443.
[7] C.F. Djuika, J. Huerta-Cepas, J.M. Przyborski, S. Deil, C.P. Sanchez, T. Doerks, P. Bork, M. Lanzer, M. Deponte, Prokaryotic ancestry and gene fusion of a dual localized peroxiredoxin in malaria parasites, Microb. Cell 2 (1) (2015) 5–13.
[8] C.F. Djuika, V. Staudacher, C.P. Sanchez, M. Lanzer, M. Deponte, Knockout of the peroxiredoxin 5 homologue PFAOP does not affect the artemisinin susceptibility of Plasmodium falciparum, Sci. Rep. 7 (1) (2017) 4410.
[9] C. Nickel, S. Rahlfs, M. Deponte, S. Koncarevic, K. Becker, Thioredoxin networks in the malarial parasite Plasmodium falciparum, Antioxid. Redox Signal 8 (7–8) (2006) 1227–1239.
[10] C.F. Djuika, S. Fiedler, M. Schnolzer, C. Sanchez, M. Lanzer, M. Deponte, Plasmodium falciparum antioxidant protein as a model enzyme for a special class of glutaredoxin/glutathione-dependent peroxiredoxins, Biochim Biophys. Acta 1830 (8) (2013) 4073–4090.
[11] V. Staudacher, C.F. Djuika, J. Koduka, S. Schlossarek, J. Kopp, M. Buchler, M. Lanzer, M. Deponte, Plasmodium falciparum antioxidant protein reveals a novel mechanism for balancing turnover and inactivation of peroxiredoxins, Free Radic. Biol. Med. 85 (2015) 228–236.
[12] L. Flohe, S. Toppo, G. Cozza, F. Ursini, A comparison of thiol peroxidase mechanisms, Antioxid. Redox Signal 15 (3) (2011) 763–780.
[13] A. Hall, K. Nelson, L.B. Poole, P.A. Karplus, Structure-based insights into the catalytic power and conformational dexterity of peroxiredoxins, Antioxid. Redox Signal 15 (3) (2011) 795–815.
[14] R. Radi, J.S. Beckman, K.M. Bush, B.A. Freeman, Peroxynitrite oxidation of sulfhydryls. The cytotoxic potential of superoxide and nitric oxide, J. Biol. Chem. 266 (7) (1991) 4244–4250.
[15] B. Morgan, D. Ezerina, T.N. Amoako, J. Riemer, M. Seedorf, T.P. Dick, Multiple glutathione disulfide removal pathways mediate cytosolic redox homeostasis, Nat. Chem. Biol. 9 (2) (2013) 119–125.
[16] M. Urscher, S.S. More, R. Alisch, R. Vince, M. Deponte, Tight-binding inhibitors efficiently inactivate both reaction centers of monomeric Plasmodium falciparum glyoxalase 1, FEBS J. 279 (14) (2012) 2568–2578.
[17] G.L. Ellman, Tissue sulfhydryl groups, Arch. Biochem. Biophys. 82 (1) (1959) 70–77.
[18] M. Trujillo, A. Clippe, B. Manta, G. Ferrer-Sueta, A. Smeets, J.P. Declercq, B. Knoops, R. Radi, Pre-steady state kinetic characterization of human peroxiredoxin 5: taking advantage of Trp84 fluorescence increase upon oxidation, Arch. Biochem. Biophys. 467 (1) (2007) 95–106.
[19] M. Hugo, L. Turell, B. Manta, H. Botti, G. Monteiro, L.E. Netto, B. Alvarez, R. Radi, M. Trujillo, Thiol and sulfenic acid oxidation of AhpE, the one-cysteine peroxiredoxin from Mycobacterium tuberculosis: kinetics, acidity constants, and conformational dynamics, Biochemistry 48 (40) (2009) 9416–9426.
[20] D. Parsonage, K.J. Nelson, G. Ferrer-Sueta, S. Alley, P.A. Karplus, C.M. Furdui, L.B. Poole, Dissecting peroxiredoxin catalysis: separating binding, peroxidation, and resolution for a bacterial AhpC, Biochemistry 54 (7) (2015) 1567–1575.
[21] R. Ogusucu, D. Rettori, D.C. Munhoz, L.E. Netto, O. Augusto, Reactions of yeast thioredoxin peroxidases I and II with hydrogen peroxide and peroxynitrite: rate constants by competitive kinetics, Free Radic. Biol. Med. 42 (3) (2007) 326–334.
[22] M. Trujillo, G. Ferrer-Sueta, R. Radi, Kinetic studies on peroxynitrite reduction by peroxiredoxins, Methods Enzymol. 441 (2008) 173–196.
[23] Y. Hayashi, I. Yamazaki, The oxidation-reduction potentials of compound I/compound II and compound II/ferric couples of horseradish peroxidases A2 and C, J. Biol. Chem. 254 (18) (1979) 9101–9106.
[24] D. Dolman, G.A. Newell, M.D. Thurlow, A kinetic study of the reaction of horseradish peroxidase with hydrogen peroxide, Can. J. Biochem. 53 (5) (1975) 495–501.
[25] Z.A. Wood, L.B. Poole, P.A. Karplus, Peroxiredoxin evolution and the regulation of hydrogen peroxide signaling, Science 300 (5619) (2003) 650–653.
[26] M. Deponte, K. Becker, Biochemical characterization of Toxoplasma gondii 1-Cys peroxiredoxin 2 with mechanistic similarities to typical 2-Cys Prx, Mol. Biochem. Parasitol. 140 (1) (2005) 87–96.
[27] M. Deponte, S. Rahlfs, K. Becker, Peroxiredoxin systems of protozoal parasites, Subcell Biochem. 44 (2007) 219–229.
[28] S.G. Rhee, I.S. Kil, Multiple functions and regulation of mammalian peroxiredoxins, Annu. Rev. Biochem. 86 (2017) 749–775.
[29] T.S. Chang, W. Jeong, S.Y. Choi, S. Yu, S.W. Kang, S.G. Rhee, Regulation of peroxiredoxin I activity by Cdc2-mediated phosphorylation, J. Biol. Chem. 277 (28) (2002) 25370–25376.
[30] T. Rabilloud, M. Heller, F. Gasnier, S. Luche, C. Rey, R. Aebersold, M. Benahmed, P. Louisot, J. Lunardi, Proteomics analysis of cellular response to oxidative stress. Evidence for in vivo overoxidation of peroxiredoxins at their active site, J. Biol. Chem. 277 (22) (2002) 19396–19401.
[31] H.H. Jang, S.Y. Kim, S.K. Park, H.S. Jeon, Y.M. Lee, J.H. Jung, S.Y. Lee, H.B. Chae,

Y.J. Jung, K.O. Lee, et al., Phosphorylation and concomitant structural changes in human 2-Cys peroxiredoxin isotype I differentially regulate its peroxidase and molecular chaperone functions, FEBS Lett. 580 (1) (2006) 351–355.
[32] H.A. Woo, S.H. Yim, D.H. Shin, D. Kang, D.Y. Yu, S.G. Rhee, Inactivation of peroxiredoxin I by phosphorylation allows localized H(2)O(2) accumulation for cell signaling, Cell 140 (4) (2010) 517–528.
[33] J.M. Lim, K.S. Lee, H.A. Woo, D. Kang, S.G. Rhee, Control of the pericentrosomal H2O2 level by peroxiredoxin I is critical for mitotic progression, J. Cell Biol. 210 (1) (2015) 23–33.
[34] J.R. Stone, S. Yang, Hydrogen peroxide: a signaling messenger, Antioxid. Redox Signal 8 (3–4) (2006) 243–270.
[35] M.R. Branco, H.S. Marinho, L. Cyrne, F. Antunes, Decrease of H2O2 plasma membrane permeability during adaptation to H2O2 in Saccharomyces cerevisiae, J. Biol. Chem. 279 (8) (2004) 6501–6506.
[36] V. Folmer, N. Pedroso, A.C. Matias, S.C. Lopes, F. Antunes, L. Cyrne, H.S. Marinho, H2O2 induces rapid biophysical and permeability changes in the plasma membrane of Saccharomyces cerevisiae, Biochim. Biophys. Acta 1778 (4) (2008) 1141–1147.
[37] F. Antunes, E. Cadenas, Estimation of H2O2 gradients across biomembranes, FEBS Lett. 475 (2) (2000) 121–126.
[38] L.C. Seaver, J.A. Imlay, Hydrogen peroxide fluxes and compartmentalization inside growing Escherichia coli, J. Bacteriol. 183 (24) (2001) 7182–7189.
[39] N. Makino, K. Sasaki, K. Hashida, Y. Sakakura, A metabolic model describing the H2O2 elimination by mammalian cells including H2O2 permeation through cytoplasmic and peroxisomal membranes: comparison with experimental data, Biochim. Biophys. Acta 1673 (3) (2004) 149–159.